Macromolecules

Article

Cite This: Macromolecules 2018, 51, 1507−1517

Stretching Dynamics of Single Comb Polymers in Extensional Flow

Danielle J. Mai,[†] Amir Saadat,[‡] Bamin Khomami,[*,‡] and Charles M. Schroeder[*,†]

[†]Department of Chemical and Biomolecular Engineering, University of Illinois at Urbana−Champaign, Urbana, Illinois 61801, United States

[‡]Material Research and Innovation Laboratory, Department of Chemical and Biomolecular Engineering, University of Tennessee, Knoxville, Tennessee 37996, United States

Supporting Information

ABSTRACT: Molecular architecture plays a key role in determining the physical properties and emergent functional properties of polymeric materials. Despite recent progress in the synthesis of structurally defined polymers, we still lack a complete understanding of how the emergent properties of topologically complex polymers arise from molecular-scale phenomena. In this work, we study the nonequilibrium dynamics of DNA-based comb polymers in extensional flow using a combination of single molecule fluorescence microscopy and Brownian dynamics (BD) simulations. In this way, we directly observe the stretching dynamics of single DNA comb polymers in planar extensional flow. Transient stretching dynamics of isolated comb polymers is studied as a function of branch density and location, branch molecular weight, and flow strength. High-fidelity BD simulations are used to provide a direct complement to single molecule experiments, providing key insights into the molecular stretching mechanisms for single combs in flow. Our results show that comb polymers stretch through fundamentally different conformational pathways compared to linear polymers. In particular, comb polymers exhibit hindered transient stretching in extensional flow, which arises due to nonlinear chain topologies. From a broad perspective, this work provides a molecular-based understanding of topologically complex polymers in flow, which could aid in the modeling and processing of advanced polymeric materials with nonlinear topologies.

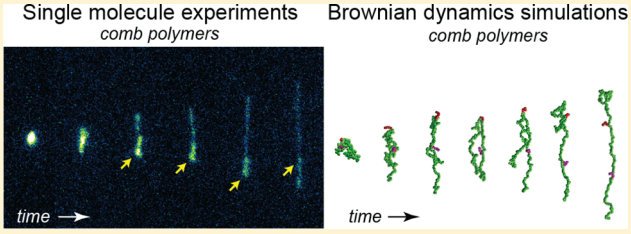

INTRODUCTION

In recent years, branched polymers have been used in a wide array of commercial applications ranging from organic electronics to membrane separations. Despite the increasing prevalence of topologically complex polymers in designing and building functional materials, we lack a complete understanding of the role of molecular architecture on the emergent physical properties of these materials.[1−4] Comb-shaped polymers and brush polymers consist of a main polymer backbone with grafted side chains known as branches or arms. This molecular architecture enables chemical and functional versatility for numerous applications, including drug delivery,[5,6] optical devices,[7] antifouling coatings,[8] renewable energy devices,[9] and desalination membranes.[10]

Comb polymers are known to exhibit more complex flow behavior compared to their linear counterparts,[1−3] including intricate linear viscoelastic signatures,[11−15] distinct stress overshoots in the startup of shear flow,[16,17] enhanced strain hardening in extensional flow,[18,19] and nonlinear stress relaxation.[19−21] Interestingly, comb polymers exhibit seemingly disparate macroscopic properties in flow, such as shear thinning (corresponding to a decrease in viscosity with increasing flow rate in shear flow) together with strain hardening (corresponding to an increase in viscosity upon increasing strain in extensional flow) for the same material. Nevertheless, these combined behaviors result in favorable processing properties for comb polymers compared to their linear analogues: shear-thinning materials can be easily extruded with lower viscosities at high shear rates,[2] whereas strain-hardening materials provide stabilized films and fibers during extensional flow processing.[22]

Given the importance of comb polymers as versatile materials in modern society, there is a clear need to understand the molecular origins of complex flow behavior and bulk-scale phenomena. Recent advances in comb polymer synthesis and purification have enabled detailed studies of the bulk rheological properties of well-defined branched polymers.[18,19,23,24] These studies have shown dramatic effects of molecular-scale architectural defects on bulk rheological properties, such that minor changes in local chain connectivity vastly impact global material response. For example, the onset of nonlinear phenomena occurs at lower flow rates for branched polymers compared to linear polymers of similar molecular weight,[18,19] with strain hardening becoming strikingly more pronounced as the branch molecular weight is increased in comb polymer melts. Although recent rheological measurements have uncovered interesting flow properties of these materials, bulk-level techniques tend to measure average properties while only indirectly inferring molecular-scale dynamics.

Received: December 30, 2017
Revised: January 25, 2018
Published: February 9, 2018

DOI: 10.1021/acs.macromol.7b02759
Macromolecules 2018, 51, 1507−1517

Single molecule techniques can be used to directly visualize the dynamics of individual polymers in flow,[25] thereby revealing distributions in molecular behavior and dynamic heterogeneity in stretching trajectories.[26−31] Over the past two decades, DNA has served as a convenient model polymer for observing the dynamics of single chains in flow,[32−36] though the vast majority of single polymer studies has mainly focused on linear chains. Recently, the dynamics of polymers with complex topologies have been studied using single molecule techniques,[4] including knotted polymers,[28,37,38] rings,[30,31,39] and branched polymers.[29] In particular, the relaxation of single tethered DNA comb polymers was studied in 2015,[29] where it was found that the precise molecular topology (number and location of side chain branches) directly impacted the longest relaxation time of the main chain backbone. However, these initial experiments only focused on surface-tethered DNA combs and did not examine polymer chain relaxation or stretching dynamics in bulk solution.

In this work, we report the direct observation of comb polymer dynamics in extensional flow using a combination of single molecule experiments and high-fidelity Brownian dynamics (BD) simulations. DNA-based comb polymers are first synthesized and characterized, followed by single molecule imaging of chain relaxation from high extension and stretching dynamics in an extensional flow generated in a microfluidic cross-slot device with feedback control (Figure 1), known as a Stokes trap.[40] Using this approach, we simultaneously visualize comb polymer backbones and branches during transient stretching in the startup of extensional flow. Our results show that isolated comb polymers stretch through fundamentally different conformational pathways compared to linear polymers. BD simulations are used to directly complement single polymer experiments. In particular, a new mesocale model for wormlike chains is developed that accurately captures backbone correlations and elasticity under high levels of fine graining. Taken together, our results show that chain architecture plays a direct role in nonequilibrium polymer dynamics, such that hindered transient stretching arises due to complex molecular topologies.

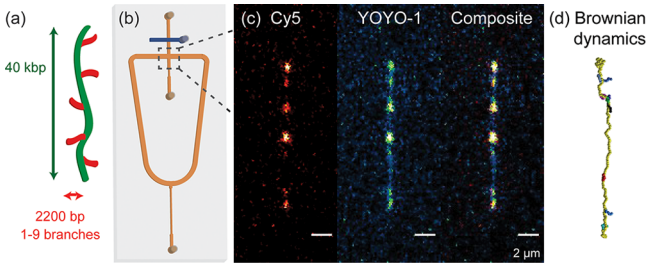

Figure 1. Stretching dynamics of single comb polymers in extensional flow. (a) Schematic showing molecular topology of DNA-based comb polymers. (b) Schematic of a microfluidic cross-slot device used to generate planar extensional flow for observing single comb polymers (orange, fluidic channels; blue, control channel). (c) Single molecule images of DNA comb polymers showing simultaneous visualization of branches (Cy5, red) and backbones (YOYO-1, green). (d) Snapshot of a single comb polymer stretching in extensional flow from BD simulations (yellow, backbone; green/red/blue, branches; 1 Kuhn step per spring).

METHODS

Synthesis and Purification of DNA Combs. DNA comb polymers were synthesized using polymerase chain reaction (PCR) and strain-promoted alkyne−azide cycloaddition (SPAAC), as previously described.[29,41] In this work, combs were synthesized with 40 kbp backbones containing either 951 bp branches or 2200 bp branches. DNA backbones were synthesized via long-range PCR using λ-phage DNA (48 502 bp) as a PCR template with incorporation of a non-natural nucleotide containing dibenzocyclooctyne (DBCO) during the reaction. In a separate PCR reaction, branches were synthesized to contain a single azide moiety at one chain terminus and internally labeled with Cy5 dye. Bulk absorbance measurements indicated that branches contained 7−8 Cy5 dyes/kbp. Linear DNA polymers (40 kbp backbones without side branches) were used as a reference to evaluate the impact of branching on dynamics.

Following synthesis and graft-onto reactions for conjugating branches to DNA backbones, gel filtration chromatography was used to remove excess branches, thereby enabling the study of optically pure comb polymers using fluorescence microscopy. A Tricorn 10/300 column was packed with Sephacryl S-1000 gel filtration media and installed on an AKTA FPLC system (GE Healthcare Life Sciences). After equilibrating the column with an aqueous buffer system (200 mM NaCl, 30 mM Tris/Tris-HCl (pH 8.0), 2 mM EDTA, filtered using 0.22 μm Millipore Stericup), SPAAC reaction products were passed through the column at a volumetric flow rate of 0.05−0.1 mL/min. Absorbance was monitored at 260 nm. The first peak to elute was identified as purified DNA comb polymer and was spin-concentrated using a Vivacon 2 column. Concentrated comb polymers were stored in 50% glycerol in elution buffer at −20 °C for up to 1 month.

Preparation of DNA Combs for Single Molecule Imaging. Linear and comb DNA polymers were fluorescently labeled by incubation with YOYO-1 (Invitrogen) at a dye-to-base-pair ratio of 1:4 in an aqueous incubation buffer (30 mM Tris/Tris-HCl, pH 8.0, 5 mM NaCl, 2 mM EDTA) for at least 1 h in the dark. Viscous imaging buffers (50−60 wt % sucrose, 30 mM Tris/Tris-HCl, pH 8.0, 5 mM NaCl, 2 mM EDTA) were prepared with an oxygen scavenging system and a reducing agent to minimize photobleaching, consisting of glucose (5 mg/mL), glucose oxidase (0.3 mg/mL), catalase (0.3 mg/mL), and β-mercaptoethanol (150 mM). Labeled DNA were diluted 50-fold into imaging buffers and rotationally mixed for at least 30 min prior to injection into a microfluidic device.

Fabrication of Microfluidic Devices. The dynamics of single comb polymers were studied in a planar extensional flow generated in a cross-slot channel geometry (Figure 1b). Two-layer microfluidic cross-slot devices were fabricated using standard techniques in soft lithography[42−44] (Supporting Information). The microdevice design includes extended inlet channels and a constriction region in the inlet channel (with 50 μm channel width), which effectively allows for working fluid pressures between 0.5 and 2.0 psi for 25−50 cP solution viscosities[45] using pressure-driven flow.

Characterization of Flow Field and Automated Hydrodynamic Trap. Pressure-driven flow was used to drive fluid through PDMS devices, thereby allowing for rapid start-up and cessation of flow. Characteristic time scales for actuating the pressure regulator to initiate or stop flow were found to be <1 s, which is significantly less than the duration of transient polymer stretching and relaxation events. Cross-slot microfluidic devices generate a planar extensional flow field near the center of the cross-slot, such that

$$v_x = -\dot{\epsilon}(x - x_0) \quad (1)$$

$$v_y = \dot{\epsilon}(y - y_0) \quad (2)$$

where v_x is velocity in the x-direction (inlet direction), v_y is fluid velocity in the y-direction (outlet direction), (x_0, y_0) is the position of the stagnation point, and $\dot{\epsilon}$ is the strain rate. The y-coordinate of the stagnation point y_0 was modulated by fine-scale adjustment of the fluid pressure in the valve control layer, which serves to alter the resistance to fluid flow in one outlet line with respect to the other. In this way, single polymers can be effectively trapped near the stagnation point for

DOI: 10.1021/acs.macromol.7b02759
Macromolecules 2018, 51, 1507−1517

long times or accumulated fluid strains ε using automated feedback control, which is implemented in a feedback loop between the imaging platform and the pressure regulator controlling pressure in the valve layer, as previously described.[30,31,43,44] Fine-scale adjustment of the stagnation point position over the range of micrometers does not appreciably change the imposed strain rate $\dot{\varepsilon}$ in the microfluidic device. Finally, strain rates were determined in cross-slot devices using particle tracking velocimetry (PTV), and particle trajectories were determined using a particle tracking algorithm[46] and ImageJ software[47] (Supporting Information).

Single Molecule Fluorescence Microscopy. Single molecule fluorescence microscopy (SMFM) was used to directly image DNA comb polymers in flow. An inverted microscope (Olympus IX-71) equipped for epifluorescence was used with a 100× oil-immersion objective lens (NA = 1.40) with 1.6× additional zoom lens and an electron multiplying charge-coupled device (EMCCD) camera (Andor iXon Ultra 897). Two-color fluorescence imaging was achieved using two continuous-wave lasers as excitation sources: a 488 nm SpectraPhysics Excelsior laser (50 mW) and a 637 nm Coherent OBIS laser (140 mW). The 488 nm optical path included absorptive neutral density filters (Thorlabs), a 488 nm long-pass dichroic mirror (ZT488rdc, Chroma), and a long-pass emission filter (BLP01-488R-25, Semrock). The intensity at the sample was ≈0.1 kW/cm^2. The 637 nm optical path includes an absorptive neutral density filter (ThorLabs), a 650 nm long-pass dichroic mirror (FF650-Di01-25×36, Semrock), and a long-pass emission filter (HQ665LP, Chroma). The intensity at the sample was ≈0.6 kW/cm^2.

For simultaneous two-color imaging of DNA combs labeled with YOYO-1 and Cy5 dyes (Figure 1c), the 488 and 637 nm optical paths were modified to include a dual-band dichroic mirror (FF500/646-Di01-25×36, Semrock) and a DualView DV2 beamsplitter apparatus with a 630 nm dichroic cube (MS-630LDX-1826, Photometrics), as shown schematically in Figure 2. The short wavelength channel was passed through a band-pass emission filter (FF01-550/88, Semrock), and the long wavelength channel was passed through band-pass (HQ700/75m, Chroma) and long-pass (HQ665LP, Chroma) emission filters. For experiments on linear DNA chains, a single color optical setup was used to include only the 488 nm laser excitation source.

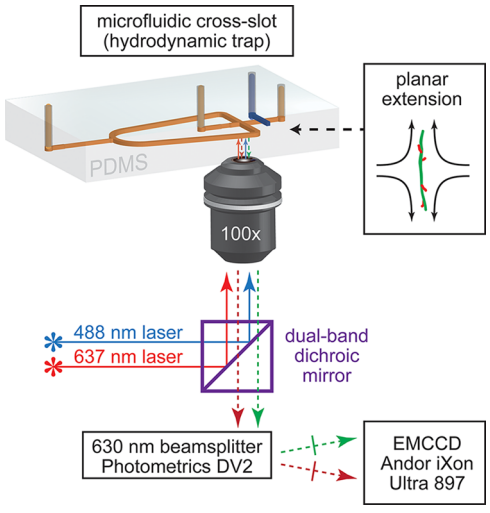

Figure 2. Schematic of optical imaging setup for simultaneous visualization of polymer backbones and side branchs. Comb polymer samples are simultaneously illuminated with 488 and 637 nm excitation sources. Comb polymer backbones (green fluorescence) and branches (red fluorescence) are visualized simultaneously by isolating fluorescence emission using a 630 nm beamsplitter (Photometrics DV2) and downstream bandpass and long-pass filters. Image channels corresponding to green (backbones) and red (branches) fluorescence emissions are acquired side-by-side on the two-dimensional image array of an EMCCD camera.

Brownian Dynamics Simulations. Brownian dynamics (BD) simulations were used to model the dynamics of single comb polymers in extensional flow (Supporting Information).[48] Semiflexible DNA molecules are modeled as bead−spring chains, where each entropic spring represents 1 Kuhn step.[48−51] This level of fine-graining represents the highest level of mesoscopic detail for coarse-grained simulations. Bead−spring chains consist of $N_{b,t}$ total beads that represent the centers of hydrodynamic resistance, connected by $N_{b,t} - 1$ massless springs that account for the entropic forces between adjacent beads. For chains with comb architectures, the number of arms (branches), the number of beads in the backbone, and the number of beads in each branch are denoted by N_a, $N_{b,bb}$, and $N_{b,ar}$, respectively. Briefly, the configurational state of the system can be specified by the position vector of all beads $\{\mathbf{r}_\mu | \mu = 1, ..., N_{b,t}\}$ or, equivalently, using the center-of-mass of the chain $\mathbf{r}_c$ and the connector vectors of all springs $\{\mathbf{Q}_k | k = 1, ..., N_{b,t} - 1\}$. The configurational evolution equation using the Itô stochastic differential equation is[48,50]

$$d\mathbf{Q} = \left\{\mathbf{K}\cdot\mathbf{Q} + \frac{1}{\zeta}\overline{\mathbf{B}}\cdot\mathbf{D}\cdot\mathbf{F}^{\phi}\right\} dt + \sqrt{\frac{2k_BT}{\zeta}}\,\overline{\mathbf{B}}\cdot\mathbf{C}\cdot d\mathbf{W} \tag{3}$$

where $\mathbf{K}$ is a $(N_{b,t} - 1) \times (N_{b,t} - 1)$ block matrix, in which the diagonal blocks are the transpose of the velocity gradient tensor $\boldsymbol{\kappa}$ and the remaining blocks are $\mathbf{0}$. In planar elongational flow

$$\boldsymbol{\kappa} = \dot{\varepsilon}\begin{pmatrix} 1 & 0 & 0 \\ 0 & -1 & 0 \\ 0 & 0 & 0 \end{pmatrix}$$

In eq 3, $\mathbf{D}$ is the diffusion tensor, $\mathbf{F}^{\phi}$ is the total conservative (nonhydrodynamic, non-Brownian) force, $\mathbf{C}$ is the coefficient tensor which is related to $\mathbf{D}$ based on the fluctuation−dissipation theorem, such that $\mathbf{D} = \mathbf{C}\cdot\mathbf{C}^T$, k_B is the Boltzmann constant, T is absolute temperature, and ζ is the friction coefficient of a bead with hydrodynamic radius a in a solvent with viscosity η_s (given by the Stokes−Einstein relation $\zeta = 6\pi\eta_s a$). In particular, the force vector $\mathbf{F}^{\phi}$ in eq 3 is composed of intramolecular bonding, bending, and excluded volume forces, such that $\mathbf{F}^{\phi} = \mathbf{F}^{spr} + \mathbf{F}^{b} + \mathbf{F}^{ev}$, where $\mathbf{F}^{spr}$ is the net spring force, $\mathbf{F}^{b}$ is the bending force, and $\mathbf{F}^{ev}$ is the non-neighboring excluded volume interaction force. $d\boldsymbol{W}$ is an increment of a 3-dimensional Wiener process. $\overline{\mathbf{B}}$ is a $(N_{b,t} - 1) \times N_{b,t}$ block matrix to convert position vectors to connector vectors, and its definition depends on molecular architecture (Supporting Information).[49,52]

A semi-implicit predictor−corrector scheme[48,51] is used to integrate eq 3 in order to obtain the internal configurations of the chains at each time step. The entropic force is modeled using the WLC-SK force relation, which allows polymer chains to be modeled by simulating 1 Kuhn step of semiflexible DNA molecules using a single spring.[53] The form of the WLC-SK force relation requires solving septic equations in the corrector steps.[48,50] Excluded volume (EV) interactions are included using a soft Gaussian potential,[54] and hydrodynamic interactions (HI) are included using the Rotne−Prager−Yamakawa tensor (Supporting Information).

Parameter Selection for BD Simulations. In BD simulations, DNA combs were parametrized in a systematic manner to match experimental conditions, with simulations incorporating intrachain HI and EV interactions. Model parameters consisted of the following parameters: contour length L_c, discretization level or number of Kuhn steps per spring ($N_{K,s} = 1$), Kuhn length b_K, HI parameter h^*, and EV parameters z^* and d^*. Table 1 summarizes the topological molecular parameters for DNA molecules comprising the backbone and arms (or branches) of the comb polymers. The contour length of natural B-form DNA is estimated using the equation $L_c = n_{bp} \times 0.34$ nm,[55] where n_{bp} is the number of base pairs. The estimated values of L_c in Table 1 account for labeling DNA with the intercalating dye YOYO-1, which is known to extend the contour length of DNA by ≈30%. The number of Kuhn steps N_K are calculated by assuming a Kuhn length b_K

DOI: 10.1021/acs.macromol.7b02759
Macromolecules 2018, 51, 1507−1517

Table 1. Molecular Properties of DNA Comb Polymer Backbones and Branches

size (bp)	L_c (μm)	N_K	R_{ee}^{θ} (μm)
40051	17.4	153	1.41
10051	3.4	30	0.62
2200	0.75	7	
951	0.32	3	

= 114 nm, which accounts for screened electrostatic interactions in the presence of sufficient salt in buffered imaging solutions.[56] The dependence of the DNA persistence length on intercalating dyes has been extensively debated, and here we assume that the persistence length is insensitive to the addition of YOYO-1.[56] The root-mean-square end-to-end distance R_{ee} of comb polymer backbones under θ-conditions can be approximated by $R_{ee}^{\theta} \approx \sqrt{N_K} b_K$.

In addition to molecular dimensions, the HI parameter h^* and EV parameters z^* and d^* were determined for DNA combs. Briefly, the HI parameter h^* dictates the strength of the intramolecular hydrodynamic interactions and can be related to the hydrodynamic bead radius (Supporting Information). Also, the EV parameters z^* and d^* are related to the magnitude and width, respectively, of the soft Gaussian EV potential between interacting beads (Supporting Information). The HI parameter h^* was determined by following a procedure initially adopted by Hsieh and Larson[57] and further applied by Saadat and Khomami.[58] In this approach, the hydrodynamic drag on a fully extended linear chain was matched to the drag for a cylindrical rod based on Batchelor's slender body theory. Assuming an effective diameter of 3 nm for double-stranded DNA and the molecular parameters in Table 1, we determined an HI parameter $h^* = 0.061$.

The EV parameters z^* and d^* were determined by considering the solvent quality. Solvent quality can be quantified using the chain interaction parameter $z = k\left(1 - \frac{T_\theta}{T}\right)\sqrt{M_w}$, where T_θ is the theta temperature and k is a numerical prefactor.[59] In BD simulations, the chain interaction parameter z can be directly related to the strength of the EV potential z^* using the relation $z = z^*\sqrt{N_b}$.[54,60] Prakash and co-workers showed that $z = 1$ results in good agreement between experiment and simulation for the equilibrium properties of λ-phage DNA at 22 °C. This value of the chain interaction parameter z is also consistent with the work of Pan et al.,[55] who estimated the chain interaction parameter z by determining the numerical prefactor k by quantitatively matching the hydrodynamic swelling ratio $\alpha_H = R_H/R_H^{\theta}$ between BD simulations and experiments. In this way, Pan et al.[55] report $k = 0.0047 \pm 0.0003$ (g/mol)$^{-1/2}$ for linear DNA molecules over a wide range of molecular weights. Subsequently, z^* can be obtained for a given level of fine graining (1 Kuhn step per spring in the current work), based on the corresponding number of DNA backbone beads. Using this approach, we determined that $z^* = 0.073$, and this value was applied to both the backbone chain and side branches, which have similar chemistry and flexibility. The EV interaction parameter d^* was chosen to minimize the sensitivity of the computed forces to d^* values, such that $d^* = (z^*)^{1/5}$.[60] It has been shown that for sufficiently long macromolecules, the choice of d^* is arbitrary and does not affect the properties of the chain.[61,62]

RESULTS AND DISCUSSION

Single Molecule Characterization of Comb Polymers.

Single molecule fluorescence microscopy was used to characterize the molecular topologies and branching densities of DNA comb polymers. The number of branches on comb polymer backbones was quantified by stretching isolated chains to high extension under strong extensional flow using the automated Stokes trap, followed by direct counting of side branches. Under these conditions, a single branch is identified as a diffraction-limited spot along the polymer backbone. Branch frequency distributions are shown in Figure 3. DNA comb polymers containing side branches with 951 bp (N_{br} = 951 bp)

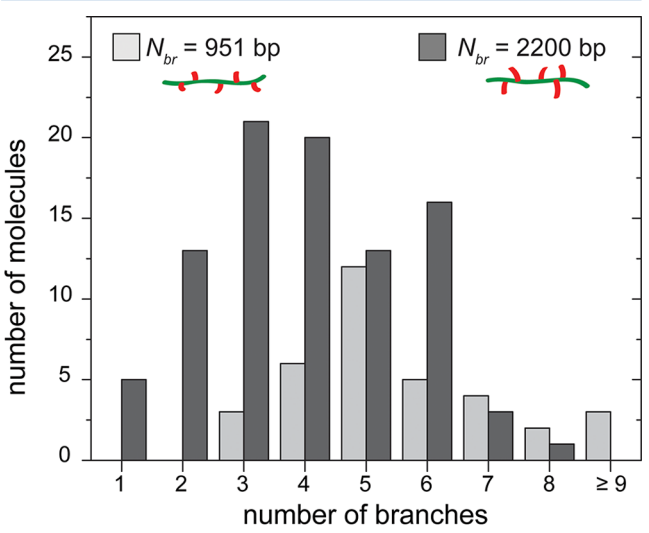

Figure 3. Branch frequency distributions for DNA-based comb polymers from single molecule imaging experiments. Branches are directly counted during high extension for single chains under strong flow.

were found to have 5.8 ± 1.8 branches, whereas comb polymers bearing side branches with 2200 bp (N_{br} = 2200 bp) had 4.1 ± 1.6 branches. In all cases, the comb or corresponding linear DNA backbone contains 40 kbp (N_{bb} = 40 kbp). These results are consistent with the notion that, on average, shorter macromolecular branches are more easily grafted onto comb polymer backbones compared to longer branches. Lower branching densities for larger branches can be attributed to increased electrostatic repulsion and steric interactions.[29,41] Branched DNA molecules in this work are considered loosely grafted combs, such that the polymer segments between branch junctions are longer than the side chains.[63,64]

The relaxation behavior of single polymers was first characterized in free solution to determine longest relaxation times of the comb or linear chain backbone τ_1. Relaxation times are determined by stretching single chains to high degrees of extension in flow, followed by flow cessation and chain relaxation under quiescent conditions. In particular, linear and comb polymers were stretched to >50% of the backbone contour length L_c in flow, followed by direct observation of chain relaxation upon cessation of flow. For these experiments, the number of branches on individual comb polymers was determined by direct counting prior to chain relaxation. Relaxation trajectories were analyzed by fitting the transient maximum polymer extension $x(t)$ to a single-exponential decay using the relation $(\langle x(t)\rangle/L_c)^2 = A\exp(-t/\tau_1) + B$, where $\langle x(t)\rangle$ is the average relaxation trajectory for an ensemble of molecules, L_c is the contour length of the backbone, and A and B are fitting constants. Relaxation data are fit over the linear entropic force regime where $\langle x(t)\rangle/L_c < 0.3$, assuming a contour length L_c = 17.4 μm for a 40 kbp DNA backbone labeled with YOYO-1 dye. The longest relaxation time for linear 40 kbp DNA is also estimated using scaling arguments as a function of solvent viscosity η and molecular weight N, such that $\tau_{1,\text{scaling}} \sim \eta N^{3\nu}$, where the effective EV exponent for DNA is taken as $\nu = 0.547$ from recent Monte Carlo simulations and bulk light scattering experiments.[45,65,66] Relaxation times are

DOI: 10.1021/acs.macromol.7b02759
Macromolecules 2018, 51, 1507−1517

estimated using a reference relaxation time for unlabeled λ-phage DNA of τ_1 = 0.063 ± 0.005 s at 1 cP.[67]

Relaxation times for comb and linear polymers from single molecule experiments ($\tau_{1,SMFM}$) and BD simulations ($\tau_{1,BD}$) are summarized in Table 2. Interestingly, we observe a clear effect of the side branches on single polymer relaxation in free solution, consistent with prior studies of branched polymers with a surface-tethered backbone chain.[29] Comb polymers generally exhibit slower relaxation behavior upon increasing branch molecular weight, even in the presence of relatively short branches. Moreover, comb polymers relax slower compared to linear chains under equivalent solution conditions, which is thought to result from increased hydrodynamic friction for bulky side branches and increased steric hindrance due to excluded volume effects. Moreover, entropic (bonded and bending) forces propagate from the branches to the backbone through grafting points, thereby generating additional relaxation modes for comb polymers.

Table 2. Longest Relaxation Time τ_1 of DNA Linear and Comb Polymers, N_{bb} = 40 kbp

N_{br} (bp)	η (cP)	$\tau_{1,scaling}$ (s)	$\tau_{1,SMFM}$ (s)	$\tau_{1,BD}$ (s)
0	25	1.8 ± 0.2	2.3 ± 0.1 (38)[a]	2.1 ± 0.3
951	25		n.d. (0)	2.2 ± 0.1
2200	25		2.4 ± 0.1 (32)	2.5 ± 0.1
0	50	3.6 ± 0.3	3.5 ± 0.8 (20)	4.2 ± 0.5
951	50		3.9 ± 0.3 (43)	4.4 ± 0.2
2200	50		5.7 ± 0.2 (19)	5.1 ± 0.2

[a]Average ± standard error of the mean; trajectory ensemble size indicated in parentheses; n = 300 trajectories for BD simulations.

The longest polymer relaxation times from BD simulations directly complement single polymer experiments. Comb relaxation dynamics are simulated using a protocol analogous to single molecule experiments, such that longest polymer relaxation times are obtained by tracking the ensemble averaged maximum extension of a polymer. We note that this analysis method includes molecular extension from both the backbone and branches; however, for the comb polymers studied in these experiments (short side branches), the maximum stretch of the backbone is essentially the same as the maximum stretch of the entire comb polymer. Overall, simulations generally show good agreement with experiments in terms of the longest relaxation time τ_1. For branched polymers, minor differences between experiments and simulations can be attributed to heterogeneity in branching density and branch placement in the underlying molecular ensembles. To simplify these effects for modeling, BD simulations generally considered comb polymers containing a given number of side branches equal to the average branching density from experiments. Unless otherwise noted, BD simulations modeled comb polymers as containing randomly distributed branch locations along the backbone chain.

BD simulations allow for the precise placement of branches along comb polymer backbones, which provides additional architectural control compared to experiments for understanding molecular-level details. Using this approach, the effect of branch position on chain relaxation in free solution was further probed using BD simulations. Here, comb polymers were generated with three branches (N_{br} = 10 kbp) placed on adjacent beads (Kuhn segments) at one location along the backbone (N_{bb} = 40 kbp). For these simulations, the relaxation of the polymer backbone extension $x_{bb}(t)$ is tracked, which effectively separates the branch contribution to relaxation dynamics. For molecular ensembles with branches placed at fractional backbone positions x_{bb}/L_c equal to 0 (backbone end), 0.25, or 0.5 (backbone center), we find τ_{bb} = 6.05, 5.39, and 4.41 ± 0.2 s, respectively (η = 50 cP, 100 trajectories per ensemble, Figure S1). Interestingly, these results reveal a dramatic slowing down of polymer backbone relaxation dynamics as branches are positioned closer to the terminus of

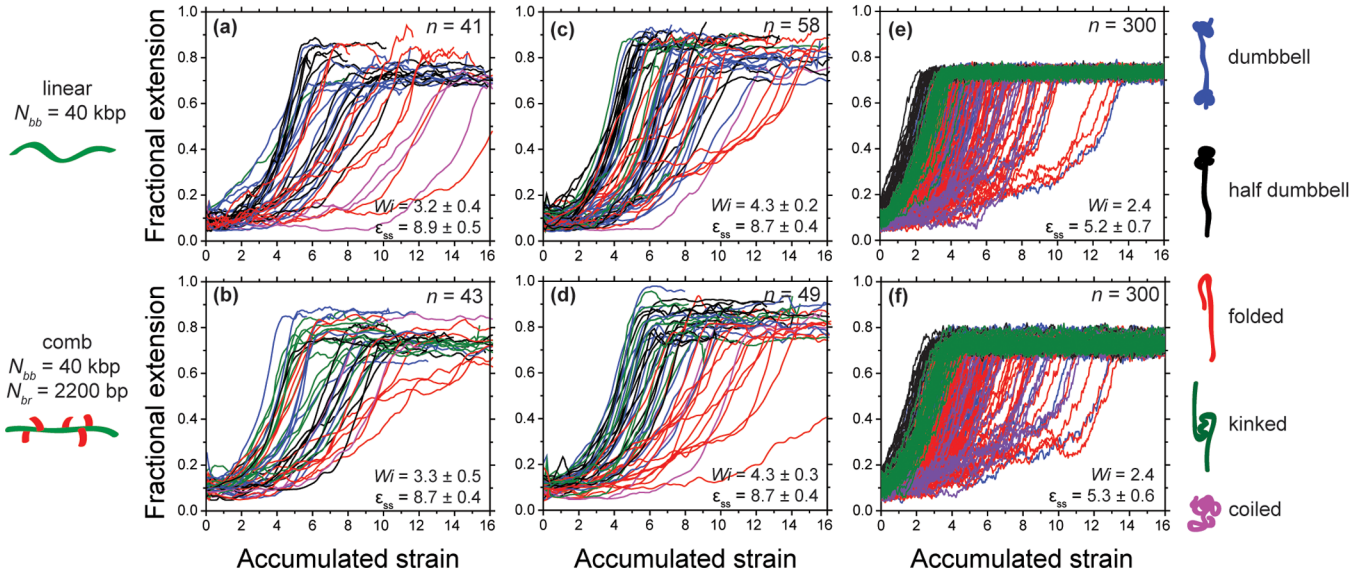

Figure 4. Transient stretching trajectories of linear DNA polymers (N_{bb} = 40 kbp) and comb polymers (N_{bb} = 40 kbp, N_{br} = 2200 bp) from single molecule experiments (a–d) and BD simulations (e, f). Transient fractional extensions x/L_c are shown as functions of accumulated fluid strain $\varepsilon = \dot{\varepsilon}t$. Trajectories for each molecular architecture are classified by flow strength (average Wi ± standard deviation) and by molecular conformation during a stretching event: dumbbell (blue), half dumbbell (black), folded (red), kinked (green), or coiled (magenta). For display, experimental trajectories are smoothed using five-point boxcar Gaussian average.

DOI: 10.1021/acs.macromol.7b02759
Macromolecules 2018, 51, 1507–1517

the backbone, which is generally consistent with observations of surface-tethered comb polymers.[29]

Stretching Dynamics of Single Comb Polymers in Flow. The transient stretching dynamics of comb polymers was studied in extensional flow, with a particular focus on the role of chain conformation and architecture on dynamics. Before the onset of flow, single polymers were thermally equilibrated for a period of at least $10\tau_1$, which ensures random initial conformations. Following the onset of flow, the maximum extension of single polymers along the extensional axis is tracked as a function of accumulated fluid strain $\varepsilon(t) = \dot{\varepsilon}t$, where t is time. Using this approach, a series of transient stretching experiments were performed on linear polymers (N_{bb} = 40 kbp) and comb polymers (N_{bb} = 40 kbp, N_{br} = 2200 bp) as a function of the dimensionless flow strength known as the Weissenberg number $Wi = \dot{\varepsilon}\tau_1$. Two subsets of experimental data corresponding to $Wi \approx 3$ and $Wi \approx 4$ are shown in Figures 4a,b and Figures 4c,d, respectively, together with corresponding BD simulation data at $Wi = 2.4$ in Figures 4e,f. In experiments, uncertainty in Wi primarily arises from statistical variations in the longest polymer relaxation time τ_1 due to branching distributions (Supporting Information).

Linear and comb polymers exhibit a pronounced degree of molecular individualism in extensional flow, wherein identical polymers adopt a diverse set of transient conformations during repeated stretching events.[26,32] In SMFM experiments, transient conformations of polymer backbones are observed by the eye and qualitatively classified as dumbbells, half dumbbells, folds, kinks, and coils,[26,32] which are sketched in Figure 4. In BD simulations, conformations are assigned at a strain of $\varepsilon = 2.0$ during the stretching process using a sorting algorithm based on relative monomer positions.[1,68] In general, we find that comb polymers adopt qualitatively similar global chain conformations during transient stretch as linear polymers. In each subplot in Figure 4, the average strain required to reach steady-state extension ε_{ss} is given for combs and linear chains chains, averaged across all conformations. Interestingly, the average values of ε_{ss} appear to be similar for linear and comb polymers at a given Wi when averaged across all conformations.

Transient stretching data in Figure 4 further show a narrowing of the spread of onset times for molecular stretching in extensional flow for comb and linear polymers in dumbbell-like conformations compared to folded and coiled conformations. For example, consider the transient molecular stretching trajectories for comb polymers in Figure 4d at $Wi \approx 4$. Comb polymers in folded conformations tend to stretch much more slowly compared to combs in dumbbell-like conformations, which is clearly observed in both single molecule experiments (Figure 4d) and BD simulations (Figure 4f). Moreover, comb polymers in dumbbell-like conformations tend to stretch with a uniform and narrow distribution of onset times. Relatively faster stretching of comb polymers in dumbbell-like conformations might be attributed to several effects, such as stiffer polymer backbones due to the presence of branches, hydrodynamically exposed polymer coils due to branch-mediated steric interactions, and increased hydrodynamic drag between the surrounding fluid and branches. As the molecular weight of the branch increases, comb polymers in folded conformations show a markedly hindered stretching behavior, which is considered in detail below.

The probabilities of transient polymer conformations for linear and comb polymers at $Wi \approx 3$ and 4 are shown in Figure 5a. These results show clear changes in the probabilities of

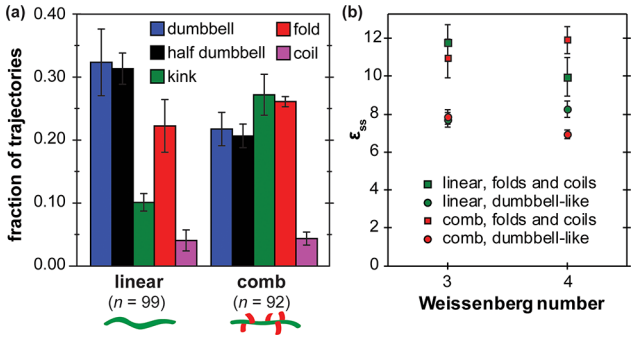

Figure 5. Role of molecular topology and conformation on transient stretching dynamics in extensional flow for linear and comb polymers. (a) Probability of molecular conformation during transient stretching events as a function of polymer architecture. For this analysis, transient stretching data at $Wi \approx 3$ and 4 are combined from trajectories shown in Figure 4. Error bars reflect standard error of the mean conformational probabilities sampled from multiple experiments. (b) Accumulated fluid strain required to reach steady-state extension ε_{ss} as a function of flow strength, molecular architecture, and molecular conformation type. Error bars represent standard error of the mean fluid strain and arise due to intrinsic stochastic variations in single molecule trajectories.

conformational stretching pathways for linear and comb polymers under the same flow conditions. In other words, even though linear and comb polymers appear to adopt similar global conformations during transient stretching in extensional flow, the relative probability of occurrence of these different conformations is vastly different for linear polymers compared to combs. In particular, comb polymers exhibit lower probabilities of dumbbell and half dumbbell conformations compared to linear chains at $Wi \approx 3$–4, whereas the probability of kinked conformations is much higher for combs. Single molecule images show that kinks tend to form near branch points, which provide points of enhanced friction along deformed chains. Specifically, 15 of 25 kinks formed near branch points rather than bare regions. The role of kinked and folded conformations are explored in detail in the following section.

Molecules adopting transient folded conformations exhibit a strong degree of dynamic heterogeneity during the stretching process. For linear chains, it is known that transient folded conformations generally show the slowest unraveling dynamics.[26] To investigate the role of polymer conformation on dynamic heterogeneity during transient stretching, we subclassified linear and comb polymers into two sets of transient molecular conformations: "dumbbell-like" (dumbbells, half dumbbells, and kinks) and "folded/coiled" conformations. For this analysis, the average strain required to reach steady-state extension ε_{ss} was determined for the dumbbell-like and folded/coiled conformations, and the values of ε_{ss} were compared for linear and comb polymers (Figure 5b). Statistical variations in ε_{ss}, shown as standard error of the mean, originate from stochastic processes during single molecule stretching trajectories. We observe a general trend that linear or comb polymers in folded conformations stretch slower on average compared to chains in dumbbell-like conformations. Dumbbell-like combs also unravel the most uniformly of all of the molecular subsets, as demonstrated by the smallest error bars shown in Figure 5b.

Finally, BD simulations were also used to understand the influence of branching on the steady-state extension of

DOI: 10.1021/acs.macromol.7b02759
Macromolecules 2018, 51, 1507–1517

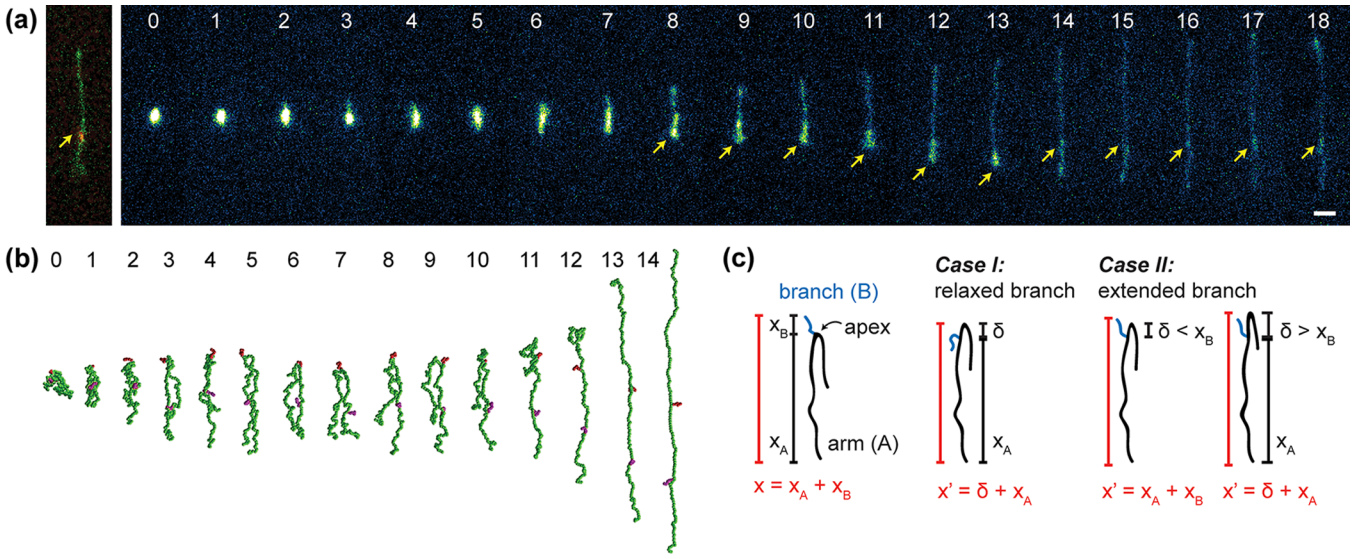

Figure 6. Hindered stretching of folded comb polymers in extensional flow. (a) Single molecule snapshots of a single comb polymer adopting a folded conformation in flow. Note that these single molecule images correspond to the bold trajectory in Figure 4d at $Wi = 4$. Two-color imaging of the stretched comb polymer indicates the presence of a branch (left-most image, branch denoted by arrow). Image 0 denotes the start of the transient extension experiment, with $\varepsilon = 1$ unit of accumulated fluid strain elapsed between successive images 0−18. Yellow arrows in images 8−18 indicate a branch that persists through the apex of the fold. Scale bar = 2.0 μm. (b) Single molecule snapshots from BD simulations show an initially folded comb polymer in planar extensional flow (green beads, backbone; red beads, branch). Each segment in the bead-spring model represents 1 Kuhn step; $\varepsilon = 1$ unit of accumulated fluid strain between successive images 0−14. (c) Schematic of hindered stretching mechanism for a comb polymers in a folded configuration.

polymers in extensional flow (Figure S2). Overall, we observe a fairly modest effect of branching on the steady-state extension of combs in extensional flow, at least for the molecular topologies and molecular weights considered in this work. Interestingly, BD simulations reveal an increase in fluctuations in steady-state polymer stretch in extensional flow as the number of branches increases (Figure S3).

Hindered Stretching of Folded Comb Polymers. Single molecule experiments reveal fundamentally different stretching mechanisms for linear and comb polymers adopting folded conformations (Figure 6). Linear polymers adopting a folded conformation generally show a smooth and slow rate of chain unraveling. For comb polymers adopting a folded conformation, we observe widely varying rates of stretching, with some molecules stretching much slower than the ensemble average. Moreover, some transient stretching trajectories include rare events in which comb polymers are caught in very slow or hindered unraveling trajectories. Interestingly, single molecule snapshots of comb polymers unraveling in a folded conformation suggest that the apex of a fold often persists near a branch point for several units of fluid strain, as shown in Figure 6a. Hindered unraveling of comb polymers in folded conformations also emerges in BD simulations, as shown in single chain snapshots (Figure 6b and Figure S4). High-resolution trajectories from BD simulations suggest that branches prevent the smooth translation of the fold apex along the backbone of the chain, thereby resulting in metastable chain conformations that unfold through a hindered mechanism.

The unraveling mechanism for a single branched polymer is shown schematically in Figure 6c. Here, a polymer chain has a single branch with extension x_B that divides the polymer backbone into two segments, with the longer segment having an instantaneous extension x_A. If the polymer develops a fold near the branch point, then the chain adopts the left-most conformation with total extension $x = x_A + x_B$. From this state, the polymer is able to continuously sample new molecular conformations in the flow field, such that conformations with total extensions $x' > x$ are favored over the initial conformation. Following this progression, two unfolding mechanisms emerge. In case I, the branch retracts as the position of the apex translates a distance δ. The total chain extension $x' = \delta + x_A$ exceeds the initial extension x, and smooth unfolding proceeds according to a similar mechanism exhibited by linear polymers. In case II, the branch remains extended while the position of the apex translates a distance $\delta < x_B$. Here, a degeneracy of conformations could exhibit the same extension $x' = x$ and are equally favored energetically. In this way, the branched polymer temporarily accommodates the fold through a series of metastable conformations, thereby hindering the unfolding process. The branched polymer only releases the fold when a conformation with $\delta > x_B$ is sampled, after which the polymer stretches to a steady-state extension.

BD simulations were employed to systematically evaluate the impact of branch position and branch molecular weight on stretching dynamics (Figure 7). Branch grafting positions were varied to change the probability of hindered unfolding events. First, comb polymers were generated with three branches at adjacent beads or Kuhn segments (N_{br} = 10 kbp) placed at fractional backbone positions x_{bb}/L_c equal to 0.25 or 0.5 (Figure 7a,b). Second, the branch length was varied for comb polymers with branches placed at the backbone center (Figure 7c,d). In all cases, 100 molecular trajectories were simulated for each branch configuration.

On the basis of these results, we found that comb polymers with long branches at the center of the backbone were most likely to adopt hindered folded conformations. Strikingly, after 10 units of accumulated strain, 21% of comb polymers with 10 kbp branches at the center retained folded conformations, in contrast to zero comb polymers with 10 kbp branches at the

DOI: 10.1021/acs.macromol.7b02759
Macromolecules 2018, 51, 1507−1517

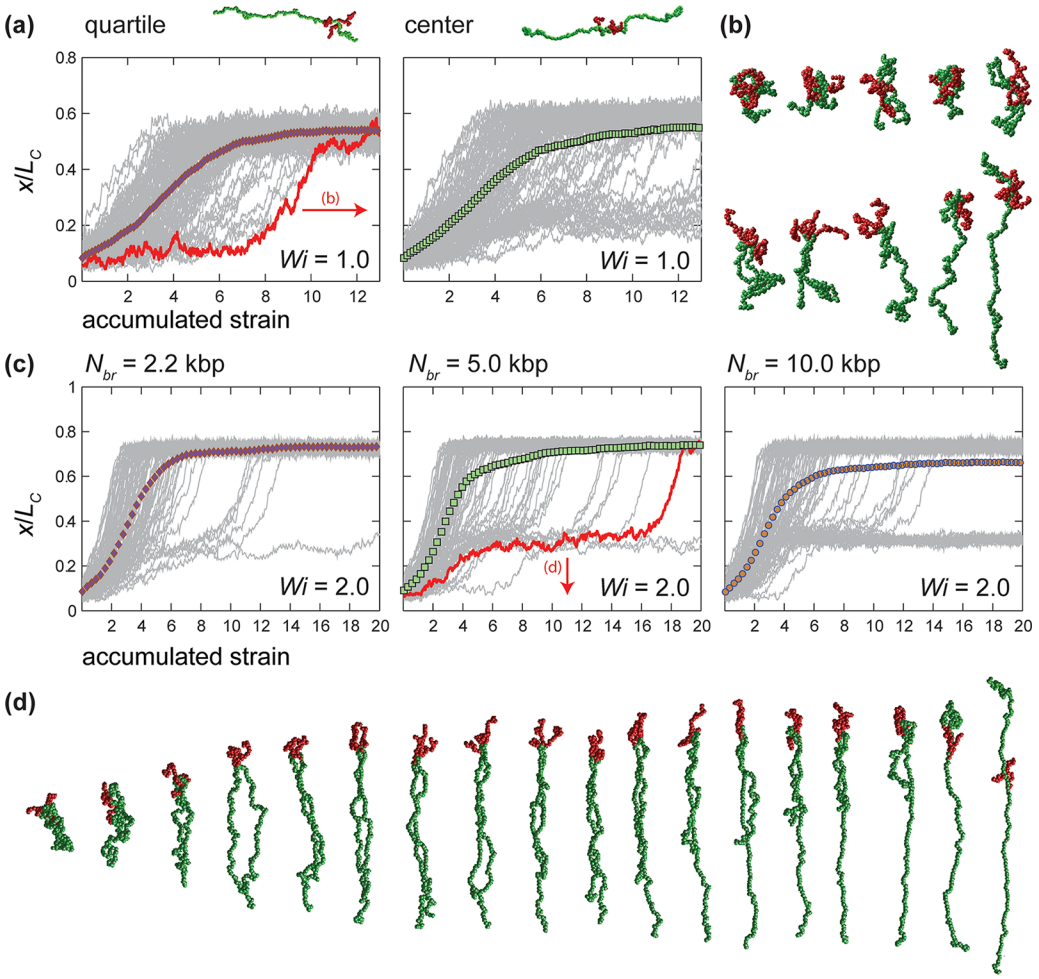

Figure 7. BD simulations demonstrate the effect of branch position and molecular weight on comb polymer stretching dynamics. (a) Fractional chain extensions x/L_c are plotted as functions of accumulated fluid strain for comb polymers with three adjacent branches (N_{br} = 10 kbp) placed at varying points along the backbone (N_{bb} = 40 kbp). Symbols represent an average across all trajectories at a given strain. (b) Snapshots of the highlighted trajectory in (a); each bead represents 1 Kuhn step; 2 strain units between snapshots. (c) x/L_c as a function of accumulated fluid strain for comb polymers with three adjacent branches of varying molecular weight (N_{br} = 2.2, 5.0, or 10.0 kbp) placed at the center of the polymer backbone (N_{bb} = 40 kbp). Symbols represent an average across all trajectories at a given strain. (d) Snapshots of the highlighted trajectory in (c); each bead represents 1 Kuhn step; 1 strain unit between snapshots.

quartile position. The persistence of folded conformations is also enhanced as the branch molecular weight increases. For comb polymers with three centered branches (N_{bb} = 40 kbp), the proportion of molecules adopting partially folded conformations after 10 units of accumulated strain increased from 0% (linear) to 6% (N_{br} = 2200 bp) to 21% (N_{br} = 10 kbp).

Based on these results, BD simulations suggest that branch position and branch molecular weight are the most critical variables in determining the unraveling dynamics of folded branched polymers. The solvent flow is not significantly affected by the presence of branches, even in the hindered unfolding cases. Here, the unraveling phase space and number of accessible polymer configurations is enlarged in the presence of side chains, as depicted in Figure 6c. The polymer backbone has a higher chance of remaining folded, resulting in a nearly frozen configuration. Taken together, SMFM experiments and BD simulations reveal that the presence of side branches in comb polymers can induce transiently hindered stretching pathways in extensional flow.

CONCLUSIONS

This work presents single molecule experiments and BD simulations of comb polymer dynamics in extensional flow. BD simulations are in good agreement with experimental results, but perhaps more importantly, the combination of these complementary approaches reveals unexpected dynamics in flow. First, our results examined the relaxation of single combs in free solution, which extends beyond prior single molecule experiments that only probed the relaxation processes for single surface-tethered comb polymers following cessation of shear flow. Our results show that comb polymers generally exhibit slower relaxation processes compared to linear chains under the same solution conditions. This effect becomes increasingly more pronounced upon increasing the size and number of side branches. Moreover, BD simulations directly show that the location and precise branching topology of comb polymers directly affects the overall relaxation process.

Our results on single comb polymer stretching dynamics reveal fundamentally different stretching mechanisms between folded linear and comb polymers. Linear polymers unravel slowly albeit smoothly from folded conformations, whereas

DOI: 10.1021/acs.macromol.7b02759
Macromolecules 2018, 51, 1507−1517

folded comb polymers can undergo unexpected hindered stretching mechanisms. Here, a comb polymer backbone accommodates a folded conformation in a transiently hindered state such that the fold apex persists near a branch point. This effect is exaggerated by increasing the branch molecular weight and positioning branches near the center of the polymer backbone.

Remarkably, these results show that inclusion of a single, local constraint (branch point) results in dramatically different global dynamic behavior of polymers. Interestingly, hindered stretching events were recently observed in linear polymer solutions with local constraints due to intermolecular interactions and nearby polymer chains (e.g., semidilute and entangled solutions).[45] In the present study, our results show that branch points provide intramolecular constraints that hinder the dynamic behavior of single comb polymers. This behavior appears to be unique to polymers with nonlinear molecular topologies, such as combs, and would have no equivalent in the case of linear polymers in dilute solutions.

Although our results reveal unexpected dynamic behavior of comb polymers at the single molecule level, the role or impact of such dynamic heterogeneity remains to be investigated in terms of bulk rheological measurements. Future work aimed at understanding the impact of dynamically heterogeneous stretching behavior and broadly distributed probabilities of polymer extension on the emergence of stress in non-equilibrium conditions would be quite interesting. Moreover, moving beyond dilute solutions, our work provides the basis for exploring the prevalence of hindered or altered molecular stretching pathways for nonlinear polymers in semidilute or concentrated solutions. From a broad perspective, our results show that conformational heterogeneities can be directly revealed using single molecule visualization of nonlinear polymer topologies during transient dynamic processes, an approach that could be used to further understand the bulk properties of materials.

■ ASSOCIATED CONTENT

Supporting Information

The Supporting Information is available free of charge on the ACS Publications website at DOI: 10.1021/acs.macromol.7b02759.

Fabrication of microfluidic devices; particle tracking velocimetry; characterization of dimensionless flow strength; Brownian dynamics simulations algorithms and methods; additional BD simulation results (Figures S1−S4) (PDF)

■ AUTHOR INFORMATION

Corresponding Authors

*E-mail: bkhomami@utk.edu (B.K.).
*E-mail: cms@illinois.edu (C.M.S.).

ORCID

Danielle J. Mai: 0000-0001-5447-2845
Charles M. Schroeder: 0000-0001-6023-2274

Present Addresses

D.J.M.: Department of Chemical Engineering, Massachusetts Institute of Technology, Cambridge, MA 02139.
A.S.: Department of Chemical Engineering, Stanford University, Stanford, CA 94305.

Author Contributions

D.J.M. and A.S. contributed equally.

Notes

The authors declare no competing financial interest.

■ ACKNOWLEDGMENTS

This work was supported by an Illinois Distinguished Fellowship and a National Science Foundation (NSF) Graduate Research Fellowship for D.J.M.; NSF Grant No. EPS-1004083 for A.S. and B.K.; and an NSF CAREER Award CBET-1254340 for C.M.S. This research was also supported in part by an allocation of advanced computational resources provided by the NSF. We thank Paul Kenis for access to cleanroom facilities, Sarah Kuhl for microdevice fabrication, and Charles E. Sing and the Schroeder group for helpful discussions.

■ REFERENCES

(1) Larson, R. G.; Hu, H.; Smith, D. E.; Chu, S. Brownian dynamics simulations of a DNA molecule in an extensional fow field. *J. Rheol.* **1999**, *43* (2), 267−304.

(2) Dealy, J. M.; Larson, R. G. *Structure and Rheology of Molten Polymers: From Structure to Flow Behavior and Back Again*; Hanser: 2006.

(3) Snijkers, F.; Pasquino, R.; Olmsted, P. D.; Vlassopoulos, D. Perspectives on the viscoelasticity and flow behavior of entangled linear and branched polymers. *J. Phys.: Condens. Matter* **2015**, *27*, 473002.

(4) Mai, D. J.; Schroeder, C. M. Single polymer dynamics of topologically complex DNA. *Curr. Opin. Colloid Interface Sci.* **2016**, *26*, 28−40.

(5) Scholz, C.; Kos, P.; Wagner, E. Comb-Like Oligoaminoethane Carriers: Change in Topology Improves pDNA Delivery. *Bioconjugate Chem.* **2014**, *25* (2), 251−261.

(6) Duro-Castano, A.; Movellan, J.; Vicent, M. J. Smart branched polymer drug conjugates as nano-sized drug delivery systems. *Biomater. Sci.* **2015**, *3*, 1321−1334.

(7) Sveinbjornsson, B. R.; Weitekamp, R. A.; Miyake, G. M.; Xia, Y.; Atwater, H. A.; Grubbs, R. H. Rapid self-assembly of brush block copolymers to photonic crystals. *Proc. Natl. Acad. Sci. U. S. A.* **2012**, *109*, 14332−14336.

(8) de Vos, W. M.; Leermakers, F. A. M.; Lindhoud, S.; Prescott, S. W. Modeling the Structure and Antifouling Properties of a Polymer Brush of Grafted Comb-Polymers. *Macromolecules* **2011**, *44* (7), 2334−2342.

(9) Chen, Y.; Thorn, M.; Christensen, S.; Versek, C.; Poe, A.; Hayward, R. C.; Tuominen, M. T.; Thayumanavan, S. Enhancement of anhydrous proton transport by supramolecular nanochannels in comb polymers. *Nat. Chem.* **2010**, *2*, 503−508.

(10) Choi, H.; Park, J.; Tak, T.; Kwon, Y. Surface modification of seawater reverse osmosis (SWRO) membrane using methyl methacrylate-hydroxy poly(oxyethylene) methacrylate (MMA-HPOEM) comb-polymer and its performance. *Desalination* **2012**, *291*, 1−7.

(11) Daniels, D. R.; McLeish, T. C. B.; Crosby, B. J.; Young, R. N.; Fernyhough, C. M. Molecular Rheology of Comb Polymer Melts. 1. Linear Viscoelastic Response. *Macromolecules* **2001**, *34* (20), 7025−7033.

(12) Kapnistos, M.; Vlassopoulos, D.; Roovers, J.; Leal, L. G. Linear Rheology of Architecturally Complex Macromolecules: Comb Polymers with Linear Backbones. *Macromolecules* **2005**, *38* (18), 7852−7862.

(13) Hu, M.; Xia, Y.; McKenna, G. B.; Kornfield, J. A.; Grubbs, R. H. Linear rheological response of a series of densely branched brush polymers. *Macromolecules* **2011**, *44*, 6935−6943.

DOI: 10.1021/acs.macromol.7b02759
Macromolecules 2018, 51, 1507−1517

(14) Inkson, N. J.; Graham, R. S.; McLeish, T. C. B.; Groves, D. J.; Fernyhough, C. M. Viscoelasticity of Monodisperse Comb Polymer Melts. *Macromolecules* **2006**, *39* (12), 4217−4227.
(15) Chambon, P.; Fernyhough, C. M.; Im, K.; Chang, T.; Das, C.; Embery, J.; McLeish, T. C.; Read, D. J. Synthesis, temperature gradient interaction chromatography, and rheology of entangled styrene comb polymers. *Macromolecules* **2008**, *41*, 5869−5875.
(16) Snijkers, F.; Vlassopoulos, D.; Lee, H.; Yang, J.; Chang, T.; Driva, P.; Hadjichristidis, N. Start-up and relaxation of well-characterized comb polymers in simple shear. *J. Rheol.* **2013**, *57*, 1079−1100.
(17) Snijkers, F.; Vlassopoulos, D.; Ianniruberto, G.; Marrucci, G.; Lee, H.; Yang, J.; Chang, T. Double Stress Overshoot in Start-Up of Simple Shear Flow of Entangled Comb Polymers. *ACS Macro Lett.* **2013**, *2* (7), 601−604.
(18) Kempf, M.; Ahirwal, D.; Cziep, M.; Wilhelm, M. Synthesis and Linear and Nonlinear Melt Rheology of Well-Defined Comb Architectures of PS and PpMS with a Low and Controlled Degree of Long-Chain Branching. *Macromolecules* **2013**, *46* (12), 4978−4994.
(19) Lentzakis, H.; Vlassopoulos, D.; Read, D. J.; Lee, H.; Chang, T.; Driva, P.; Hadjichristidis, N. Uniaxial extensional rheology of well-characterized comb polymers. *J. Rheol.* **2013**, *57*, 605−625.
(20) Kirkwood, K. M.; Leal, L. G.; Vlassopoulos, D.; Driva, P.; Hadjichristidis, N. Stress Relaxation of Comb Polymers with Short Branches. *Macromolecules* **2009**, *42* (24), 9592−9608.
(21) Lee, J. H.; Driva, P.; Hadjichristidis, N.; Wright, P. J.; Rucker, S. P.; Lohse, D. J. Damping behavior of entangled comb polymers: experiment. *Macromolecules* **2009**, *42*, 1392−1399.
(22) McLeish, T. A tangled tale of topological fluids. *Phys. Today* **2008**, *61* (8), 40.
(23) van Ruymbeke, E.; Lee, H.; Chang, T.; Nikopoulou, A.; Hadjichristidis, N.; Snijkers, F.; Vlassopoulos, D. Molecular rheology of branched polymers: decoding and exploring the role of architectural dispersity through a synergy of anionic synthesis, interaction chromatography, rheometry and modeling. *Soft Matter* **2014**, *10*, 4762−4777.
(24) Snijkers, F.; Kirkwood, K.; Vlassopoulos, D.; Leal, L.; Nikopoulou, A.; Hadjichristidis, N.; Coppola, S. Viscoelasticity and nonlinear simple shear flow behavior of an entangled asymmetric exact comb polymer solution. *J. Rheol. (Melville, NY, U. S.)* **2016**, *60*, 451−463.
(25) Schroeder, C. M. Single polymer dynamics for molecular rheology. *J. Rheol.* **2018**, *62*, 371−403.
(26) Smith, D. E.; Chu, S. Response of Flexible Polymers to a Sudden Elongational Flow. *Science* **1998**, *281*, 1335−1340.
(27) Schroeder, C. M.; Babcock, H. P.; Shaqfeh, E. S. G.; Chu, S. Observation of Polymer Conformation Hysteresis in Extensional Flow. *Science* **2003**, *301*, 1515−1519.
(28) Renner, C. B.; Doyle, P. S. Stretching self-entangled DNA molecules in elongational fields. *Soft Matter* **2015**, *11*, 3105−3114.
(29) Mai, D. J.; Marciel, A. B.; Sing, C. E.; Schroeder, C. M. Topology-Controlled Relaxation Dynamics of Single Branched Polymers. *ACS Macro Lett.* **2015**, *4*, 446−452.
(30) Li, Y.; Hsiao, K. W.; Brockman, C. A.; Yates, D. Y.; Robertson-Anderson, R. M.; Kornfield, J. A.; San Francisco, M. J.; Schroeder, C. M.; McKenna, G. B. When Ends Meet: Circular DNA Stretches Differently in Elongational Flows. *Macromolecules* **2015**, *48*, 5997−6001.
(31) Hsiao, K.-W.; Schroeder, C. M.; Sing, C. E. Ring Polymer Dynamics Are Governed by a Coupling between Architecture and Hydrodynamic Interactions. *Macromolecules* **2016**, *49*, 1961−1971.
(32) Perkins, T. T.; Smith, D. E.; Chu, S. Single Polymer Dynamics in an Elongational Flow. *Science* **1997**, *276*, 2016−2021.
(33) Shaqfeh, E. S. The dynamics of single-molecule DNA in flow. *J. Non-Newtonian Fluid Mech.* **2005**, *130*, 1−28.
(34) Latinwo, F.; Schroeder, C. M. Model systems for single molecule polymer dynamics. *Soft Matter* **2011**, *7*, 7907−7913.
(35) Brockman, C.; Kim, S. J.; Schroeder, C. M. Direct observation of single flexible polymers using single stranded DNA. *Soft Matter* **2011**, *7*, 8005−8012.
(36) Mai, D. J.; Brockman, C.; Schroeder, C. M. Microfluidic systems for single DNA dynamics. *Soft Matter* **2012**, *8*, 10560−10572.
(37) Klotz, A. R.; Narsimhan, V.; Soh, B. W.; Doyle, P. S. Dynamics of DNA Knots during Chain Relaxation. *Macromolecules* **2017**, *50*, 4074−4082.
(38) Narsimhan, V.; Klotz, A. R.; Doyle, P. S. Steady-State and Transient Behavior of Knotted Chains in Extensional Fields. *ACS Macro Lett.* **2017**, *6*, 1285−1289.
(39) Robertson, R. M.; Laib, S.; Smith, D. E. Diffusion of isolated DNA molecules: Dependence on length and topology. *Proc. Natl. Acad. Sci. U. S. A.* **2006**, *103*, 7310−7314.
(40) Shenoy, A.; Rao, C. V.; Schroeder, C. M. Stokes trap for multiplexed particle manipulation and assembly using fluidics. *Proc. Natl. Acad. Sci. U. S. A.* **2016**, *113*, 3976−3981.
(41) Marciel, A. B.; Mai, D. J.; Schroeder, C. M. Template-Directed Synthesis of Structurally Defined Branched Polymers. *Macromolecules* **2015**, *48*, 1296−1303.
(42) Unger, M. A.; Chou, H.-P.; Thorsen, T.; Scherer, A.; Quake, S. R. Monolithic microfabricated valves and pumps by multilayer soft lithography. *Science* **2000**, *288*, 113−116.
(43) Tanyeri, M.; Ranka, M.; Sittipolkul, N.; Schroeder, C. M. A microfluidic-based hydrodynamic trap: design and implementation. *Lab Chip* **2011**, *11*, 1786−1794.
(44) Tanyeri, M.; Schroeder, C. M. Manipulation and confinement of single particles using fluid flow. *Nano Lett.* **2013**, *13*, 2357−2364.
(45) Hsiao, K.-W.; Sasmal, C.; Prakash, J. R.; Schroeder, C. M. Direct observation of DNA dynamics in semidilute solutions in extensional flow. *J. Rheol.* **2017**, *61*, 151−167.
(46) Sbalzarini, I. F.; Koumoutsakos, P. Feature point tracking and trajectory analysis for video imaging in cell biology. *J. Struct. Biol.* **2005**, *151*, 182−195.
(47) Schneider, C. A.; Rasband, W. S.; Eliceiri, K. W. NIH Image to ImageJ: 25 years of image analysis. *Nat. Methods* **2012**, *9*, 671−675.
(48) Saadat, A.; Khomami, B. Computationally efficient algorithms for incorporation of hydrodynamic and excluded volume interactions in Brownian dynamics simulations: A comparative study of the Krylov subspace and Chebyshev based techniques. *J. Chem. Phys.* **2014**, *140*, 184903.
(49) Bird, R. B.; Curtiss, C. F.; Armstrong, R. C.; Hassager, O. *Dynamics of Polymeric Liquids*, 2nd ed.; Wiley: New York, 1987; Vol. 2.
(50) Öttinger, H. C. *Stochastic Processes in Polymeric Fluids*; Springer-Verlag: Berlin, 1996.
(51) Somasi, M.; Khomami, B.; Woo, N. J.; Hur, J. S.; Shaqfeh, E. S. Brownian dynamics simulations of bead-rod and bead-spring chains: numerical algorithms and coarsegraining issues. *J. Non-Newtonian Fluid Mech.* **2002**, *108*, 227−255.
(52) Lee, Y. M.; Joo, Y. L. Brownian dynamics simulations of star-branched polymers in dilute solutions in extensional flow. *J. Non-Newtonian Fluid Mech.* **2006**, *140*, 71−86. Special Issue on the {XIVth} International Workshop on Numerical Methods for Non-Newtonian Flows, Santa Fe, 2005XIVth International Workshop on Numerical Methods for Non-Newtonian Flows, Santa Fe, 2005.
(53) Saadat, A.; Khomami, B. A new bead-spring model for simulation of semi-flexible macromolecules. *J. Chem. Phys.* **2016**, *145*, 204902.
(54) Prakash, J. R.; Öttinger, H. C. Viscometric Functions for a Dilute Solution of Polymers in a Good Solvent. *Macromolecules* **1999**, *32*, 2028−2043.
(55) Pan, S.; Ahirwal, D.; Nguyen, D. A.; Sridhar, T.; Sunthar, P.; Prakash, J. R. Viscosity Radius of Polymers in Dilute Solutions: Universal Behavior from DNA Rheology and Brownian Dynamics Simulations. *Macromolecules* **2014**, *47* (21), 7548−7560.
(56) Kundukad, B.; Yan, J.; Doyle, P. S. Effect of YOYO-1 on the mechanical properties of DNA. *Soft Matter* **2014**, *10*, 9721−9728.
(57) Hsieh, C. C.; Larson, R. G. Modeling hydrodynamic interaction in Brownian dynamics: Simulations of extensional and shear flows of

DOI: 10.1021/acs.macromol.7b02759
Macromolecules 2018, 51, 1507−1517

dilute solutions of high molecular weight polystyrene. *J. Rheol.* **2004**, *48*, 995−1021.
(58) Saadat, A.; Khomami, B. Molecular based prediction of the extensional rheology of high molecular weight polystyrene dilute solutions: A hi-fidelity Brownian dynamics approach. *J. Rheol.* **2015**, *59*, 1507−1525.
(59) Rubinstein, M.; Colby, R. H. In *Polymer Physics*; York, N., Ed.; Oxford University Press: 2003.
(60) Kumar, K. S.; Prakash, J. R. Equilibrium Swelling and Universal Ratios in Dilute Polymer Solutions: Exact Brownian Dynamics Simulations for a Delta Function Excluded Volume Potential. *Macromolecules* **2003**, *36*, 7842−7856.
(61) Prabhakar, R.; Prakash, J. R.; Sridhar, T. A successive fine-graining scheme for predicting the rheological properties of dilute polymer solutions. *J. Rheol.* **2004**, *48*, 1251−1278.
(62) Sunthar, P.; Prakash, J. R. Parameter-Free Prediction of DNA Conformations in Elongational Flow by Successive Fine Graining. *Macromolecules* **2005**, *38*, 617−640.
(63) Daniel, W. F. M.; Burdyńska, J.; Vatankhah-Varnoosfaderani, M.; Matyjaszewski, K.; Paturej, J.; Rubinstein, M.; Dobrynin, A. V.; Sheiko, S. S. Solvent-free, supersoft and superelastic bottlebrush melts and networks. *Nat. Mater.* **2016**, *15*, 183.
(64) Paturej, J.; Sheiko, S. S.; Panyukov, S.; Rubinstein, M. Molecular structure of bottlebrush polymers in melts. *Sci. Adv.* **2016**, *2*, e1601478.
(65) Tree, D. R.; Muralidhar, A.; Doyle, P. S.; Dorfman, K. D. Is DNA a Good Model Polymer? *Macromolecules* **2013**, *46*, 8369−8382.
(66) Pan, S.; Nguyen, D. A.; Sridhar, T.; Sunthar, P.; Prakash, J. R. Universal solvent quality crossover of the zero shear rate viscosity of semidilute DNA solutions. *J. Rheol.* **2014**, *58*, 339−368.
(67) Perkins, T.; Quake, S.; Smith, D.; Chu, S. Relaxation of a single DNA molecule observed by optical microscopy. *Science* **1994**, *264*, 822−826.
(68) Venkataramani, V.; Sureshkumar, R.; Khomami, B. Coarse-grained modeling of macromolecular solutions using a configuration-based approach. *J. Rheol.* **2008**, *52*, 1143−1176.

DOI: 10.1021/acs.macromol.7b02759
Macromolecules 2018, 51, 1507−1517